LANGMUIR Article
Cite This: Langmuir XXXX, XXX, XXX−XXX
pubs.acs.org/Langmuir

Silk Molecular Weight Influences the Kinetics of Enzymatically Cross-linked Silk Hydrogel Formation

A. Pasha Tabatabai,[†,‡] Benjamin P. Partlow,[§] Nicole R. Raia,[§] David L. Kaplan,[§] and Daniel L. Blair*[,†,‡]

[†]Department of Physics, Georgetown University, Washington, District of Columbia 20057, United States
[‡]Institute for Soft Matter Synthesis and Metrology, Georgetown University, Washington, District of Columbia 20057, United States
[§]Department of Biomedical Engineering, Tufts University, Medford, Massachusetts 02155, United States

Supporting Information

ABSTRACT: We transform reconstituted silk solutions into robust hydrogels through covalent dityrosine cross-linking resulting from an enzymatic reaction. The bulk rheological properties and the covalent dityrosine bond formation of these gels are measured during polymerization. We compare the time-resolved bond formation to the mechanical properties, where we find that the gelation process is consistent with a model of percolation. The molecular weight of the protein determines whether a secondary mode of growth postpercolation exists, indicating that molecular weight changes affect the mechanisms by which these gels polymerize.

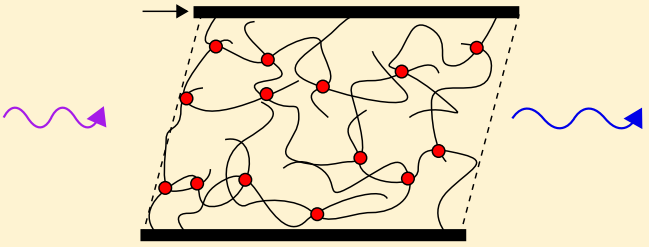

INTRODUCTION

Understanding and creating biologically compatible substrates in vitro is crucial to making progress toward the design of new cell scaffolds for tissue engineering.[1,2] Hydrogels make ideal scaffolds because they form hydrated three-dimensional networks and can be designed to be strong and biocompatible.[3,4] When designing hydrogels, it is necessary to have tunable network features like the modulus,[5] which is often measured through bulk rheology and is a consequence of the chemistry of the constituent polymer building blocks of the network.[6,7]

Hydrogels can be formed from either natural biopolymers or synthetic alternatives.[8−12] Polymers are chosen or designed with covalent-bonding sites at specific locations along the polymer, and control of bonding at these sites determines the final architecture and mechanical properties of the hydrogel. Often times, the fully polymerized hydrogel structure is observed through electron microscopy or inferred from bulk rheology. However, simply focusing on the final structure omits the kinetic pathway by which the gel polymerizes; to fully optimize the design of hydrogels, it is important to know the final architecture and the order by which the architecture is achieved a priori.[13,14]

In this work, we utilize a silk protein-based system in which bulk rheological properties and covalent bond formation are directly measured during polymerization. We focus on the kinetics as a way to understand the mechanisms of gelation. Differences between bond formation and modulus growth indicate changes in the polymerization mechanisms, providing insight into the relevant processes of hydrogel formation.

The hydrogels in this study are made by enzymatically cross-linking reconstituted silk fibroin protein. Reconstituted silk fibroin solutions make ideal hydrogels that are tunable, biocompatible, and promote cell viability.[15−18] Covalent bonding between two tyrosine residues through an enzymatic mechanism forms a network with specific and permanent cross-linking.[15] The fluorescence of individual tyrosine residues and covalently cross-linked dityrosines differs, allowing us to directly monitor the bond formation with optical techniques. The ability to measure covalent bonding and bulk properties during network formation provides an opportunity to understand how changes in silk hydrogel constituents manifest themselves on the macroscopic and microscopic scales. We create two different molecular weight distributions of silk protein fragments with peak molecular weights of 340 and 110 kDa to test the effects of molecular weight on polymerization kinetics. A comparison between the gelation of the two different molecular weight distributions reveals that molecular weight nontrivially affects the kinetics of the hydrogel formation.

METHOD

Bombyx mori silk cocoons are reconstituted following the protocol outlined by Rockwood et al.[19] Briefly, fibroin protein is isolated from cocoons after degumming in 0.02 M aqueous sodium carbonate to remove the sericin protein. We create two different molecular weight (MW) distributions of protein by

Received: September 8, 2018
Revised: November 1, 2018
Published: November 13, 2018

DOI: 10.1021/acs.langmuir.8b02950
Langmuir XXXX, XXX, XXX−XXX

adjusting the degumming time.[20] The two MW distributions are defined by their peak MWs of 340 and 110 kDa, which are created by degumming steps of 10 and 120 min, respectively. The shapes of these molecular weight distributions have been previously determined by Partlow et al.[20] Once degumming is complete, fibroin protein is solubilized by denaturation in 9.3 M aqueous lithium bromide for 4 h, and dialysis is performed with a 3.5 kDa molecular weight cutoff membrane to remove the lithium bromide ions from solution.

Silk solutions are mixed with horseradish peroxidase (HRP) enzymes and hydrogen peroxide (H_2O_2). The HRP uses H_2O_2 as a fuel to form free radicals from tyrosines on the silk protein.[21,22] Two free radical tyrosines combine to form a covalent dityrosine bond, creating either an intra- or interprotein cross-link. Dityrosine bonds have unique fluorescence spectra that are separate from individual tyrosine fluorescence; dityrosine bonds are excited at 315 nm and the intensity of fluoresced light at 425 nm (F) is collected and proportional to the number of dityrosine bonds.[23,24] We keep the concentration of HRP constant at 10 units mL^{-1}, and H_2O_2 concentrations are kept at 0.005% unless otherwise mentioned. The mass concentration of silk (c) is varied.

Solutions containing silk, HRP, and H_2O_2 are mixed and immediately loaded into either a fluorescent plate reader or a rheometer in which polymerization is monitored. For rheological measurements, an oscillatory strain amplitude of 1% and frequency of 1 Hz is used; these values correspond to the linear regime of the fully formed gel (Figure S1). We use fixed frequency and fixed strain measurements as a practical tool for hydrogel design. Alternatively, the dynamic viscoelastic spectra can be measured.[13,14] The storage modulus (G'), the loss modulus (G''), and the normal force are recorded every 30 s during polymerization. In fluorescence experiments, the intensity of fluoresced light is recorded every 30 s.

Because fibroin's amino acid sequence has low complexity and is very repetitive, 340 and 110 kDa proteins have similar chemistries and equivalent densities of tyrosines.[25,26] The chemical reconstitution process results in unstructured random-coil protein despite the propensity for ordered β-sheets that are observed in spun fibers.[27,28] As a consequence, the chemical reconstitution minimizes the possibility that hydrophobic tyrosines are folded into secondary structure and inaccessible for cross-linking. Small-angle neutron scattering shows that the Porod exponent of the protein is within 10% of the Porod exponent for a polymer in a θ-solvent.[28] Given that the polydispersity of each molecular weight distribution is large, we use θ-solvent scaling to conveniently approximate the radius of gyration R_G = 7.0 nm for 340 kDa protein and R_G = 4.5 nm for 110 kDa protein.[20,29] Estimates for the overlap concentration c^* are calculated by $c^* = 3\ \mathrm{MW}/4\pi R_G^3 N_A$, where N_A is Avogadro's constant, in the range from 40 to 70 mg mL^{-1} for 340 and 110 kDa proteins, respectively. Additionally, the small-angle neutron scattering measurements of the 340 kDa protein provide a smaller value of R_G = 4.0 nm due to an averaging over the entire molecular weight distribution.[28] Therefore, the use of R_G = 7.0 nm and 4.5 nm for the 340 and 110 kDa protein produces a conservative lower limit on c^*; all the measurements are performed in the dilute regime, where $c < c^*$. All the values of c for a given MW are drawn from the same stock and therefore have identical molecular weight distributions. It has been previously shown that the fragmentation induced by reconstitution occurs effectively randomly; therefore, we do not expect that the different molecular weight distributions have different propensities for the localization of tyrosines near fragment ends.[20]

RESULTS AND DISCUSSION

Characteristic polymerization curves for both the 340 and 110 kDa protein gels in Figure 1a show that $G'(t)$ depends on

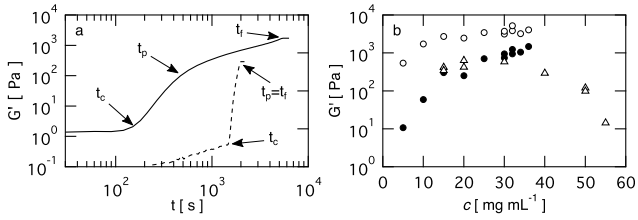

Figure 1. (a) Representative polymerization curve of $G'(t)$ with time scales t_c, t_p, and t_f defined for 340 kDa (solid line) and 110 kDa (dashed line) gels. (b) $G'(t_f)$ (○) and $G'(t_p)$ (●) for 340 kDa and $G'(t_f)$ (△) for 110 kDa gels as a function of c.

MW; discussion of the relationship between G' and G'' is available in the Supporting Information. The interpretation of $G'(t)$ requires us to define three important time scales, which are indicated in Figure 1: the critical time t_c, the percolation time t_p, and the final time t_f. Both 340 and 110 kDa protein gels exhibit a delay period where the system is still a fluid for $t < t_c$; G' increases after t_c. In 340 kDa gels, $G'(t > t_c)$ is interpreted through two separate modes of growth occurring for $t_c \leq t < t_p$ and $t_p \leq t < t_f$. However, 110 kDa gels polymerize through only one mode when $t > t_c$. When a secondary mode of growth exists, $G''(t)$ experiences a local maximum around $t = t_p$. These features of $G'(t)$, as well as the relationship between G' and G'' and the normal force during polymerization, are robust and occur for all measured concentrations (Figures S2 and S3).

At $t = t_f$, G' reaches a plateau and $G'(t_f)$ increases with c in the 340 kDa gels, whereas $G'(t_f)$ depends nonmonotonically on c in the 110 kDa gels (Figures 1b and S4). The range of c used is determined by the time scale for gelation; gels do not form when c is too low and form too quickly to be measured if c is too high. The range of measurable concentrations depends on the molecular weight distribution. Therefore, it is unclear if a similar drop in $G'(t_f)$ would be observed in 340 kDa gels if c is further increased.

Despite the nonlinear evolution of $G'(t)$, the fluorescence $F(t)$ during gelation grows linearly for $t > 0$ until F plateaus when covalent bonds stop forming at $t = t_b$ (Figure 2). Linear bond growth is seen for both 340 and 110 kDa gels, and the maximum fluorescence $F(t_b)$ increases with c and plateaus for both MW distributions. F is proportional to the number of

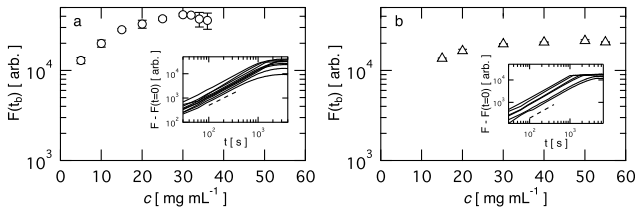

Figure 2. Maximum fluorescence $F(t_b)$ as a function of c for (a) 340 and (b) 110 kDa gels. Error bars are the standard deviation of four independent trials. Insets show the growth of fluorescence $F - F(t = 0)$ for both MW gels and dashed lines are a slope of 1.0.

DOI: 10.1021/acs.langmuir.8b02950
Langmuir XXXX, XXX, XXX−XXX

covalent bonds, including both bonds that are incorporated into the load-bearing network and spurious bonds such as loops and dangling ends. The peak in $G''(t_p)$ for high-MW gels suggests the existence of these nonload-bearing structures (Figure S2). Because $F(t_b)$ is slightly higher in the 340 kDa gels than in the 110 kDa gels at a given value of c, the former have a higher density of dityrosine bonds and more covalent bonds per protein.

Detailed interpretations of the physical basis of the different time regimes (t_c, t_p, t_f, and t_b) are presented in the following subsections.

Aggregation of Both Molecular Weight Distributions are Similar in the Fluid Phase: $t < t_c$. For $t < t_c$, the system is a fluid. Although a measurable, and sometimes increasing, value of $G'(t < t_c)$ is shown in Figure 1, similar effects are seen in solutions containing only the silk protein (data not shown). Therefore, nonzero values of $G'(t < t_c)$ are attributed to the interfacial effects and have been previously observed in protein suspensions.[20,30,31]

Covalent bonds are being created at a constant rate of $t > 0$, suggesting that aggregates are nucleating for $t < t_c$ (Figure 2). Eventually, the aggregate size grows until a system spanning aggregate forms at $t = t_c$, causing a significant growth in G'. The scaling of $t_c \propto c^{-1}$ for both MW is consistent with the Smoluchowski doubling time, suggesting that the details of aggregate formation are similar in both cases (Figure 3).[32]

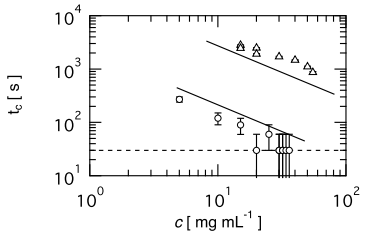

Figure 3. Scaling of t_c with c for 340 kDa (○) and 110 kDa (△) gels. Solid lines have a slope of −1.0, the dashed line is the time resolution of the measurement, and error bars correspond to the 30 s measurement interval.

Insights in the covalent bonding for $t < t_c$ are found by further investigating the final values of $G'(t_f)$ seen in Figure 1b. The nonmonotonic dependence of $G'(t_f)$ on c in 110 kDa gels is minimized/removed when the concentration of H_2O_2 is increased (Figure S4). Therefore, the drop in $G'(t_f)$, indicating the formation of a weaker network despite the addition of more protein, is a consequence of depleted H_2O_2. Consequently, we suggest that intraprotein cross-links form first, only creating interprotein bonds with surplus H_2O_2. When increasing c, more H_2O_2 is utilized for intraprotein bonds and the connectivity of the network suffers. This is consistent with these solutions being in the dilute phase ($c < c^*$), and that free radical tyrosines must associate to form a dityrosine bond; in the dilute phase, tyrosines are more likely to come into contact with another tyrosine on the same chain through thermal fluctuations than by the diffusion of the entire protein. Despite the ability to adjust the concentration of H_2O_2, we do not compare the kinetics of the different fuel levels because the enzyme catalysis rate also depends on H_2O_2.[33] Additionally, the rate of bond formation is independent of H_2O_2, consistent with previous work.[34]

Percolation Drives Initial Modulus Growth: $t_c \leq t < t_p$. Once a network-spanning aggregate is formed at $t = t_c$, the system is a solid. We quantify changes in the modulus associated with the bulk properties independent of interfacial effects by defining $\Delta G = G' - G'(t_c)$. When $t_c \leq t < t_p$, $\Delta G \sim \Delta t^{\alpha_1}$, where $\Delta t = (t - t_c)$, for both MW gels (Figure 4). The values of α_1 fluctuate around $\alpha_1 = 2$ for the 340 kDa gels and range between $2 < \alpha_1 < 3.5$ for the 110 kDa gels (Figure 5).

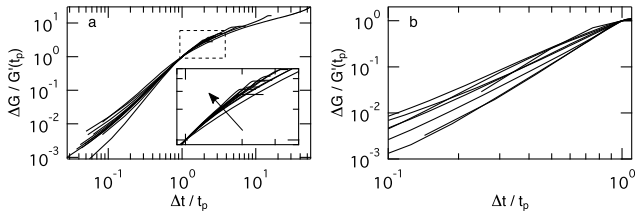

Figure 4. Rescaled moduli growth ΔG as a function of Δt shifted by $G'(t_p)$ and t_p for comparison among different values of c. (a) The 340 kDa gels at c = 5, 10, 15, 20, 25, 30, 32, 34, and 36 mg mL^{-1}. Inset is a magnification of the dashed box with an arrow indicating increasing c. (b) The 110 kDa gels at c = 15, 20, 30, 40, 50, and 55 mg mL^{-1}.

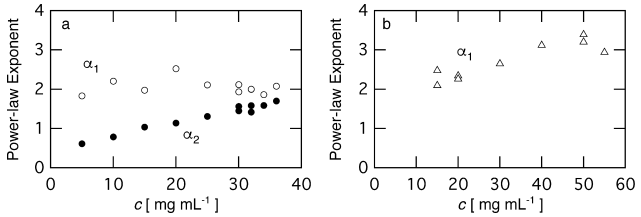

Figure 5. Power-law exponents α_1 and α_2, calculated from fits to the data in Figure 4, for 340 (a) and 110 kDa (b) gels as functions of c.

We define the bond fraction p as the probability that a bond is formed between two molecules with the critical number of bonds p_c such that at $p = p_c$, a network-spanning cluster is formed; the system is a liquid for $p < p_c$. We observe that values of α_1 are consistent with Rouse-like percolation when we make the approximation that $(p - p_c) \sim (t - t_c) \sim \Delta t$, motivated by the linear bond growth in Figure 2[35] Although these gels started as dilute solutions of proteins ($c < c^*$), we expect that the introduction of Rouse-like dynamics occurs as a consequence of transitioning into a system-spanning network. This is further supported by the evolution of $G''(t)$ (Figure S2).

The modulus growth for $t_c \leq t < t_p$ is consistent with Rouse-like percolation; over the range of silk concentrations for which the 340 and 110 kDa gels can both be measured, the moduli $G'(t_p)$ are roughly equivalent between the two MW distributions (Figure 1b). Taking the approximation for the mesh size $\xi \approx (k_B T/G')^{1/3}$, where k_B is Boltzmann constant, T is the temperature, G' is converted into a characteristic length scale. For c = 30 mg mL^{-1}, $G'(t_p) \approx 400$ Pa, resulting in $\xi \approx 20$ nm, which is equivalent to roughly the diameter of the protein $2 \times R_G$. Therefore, both MW gels have mesh sizes equivalent to the protein size after Rouse-like percolation.

Secondary Growth Drives Subprotein Length Scale Aggregation: $t_p \leq t < t_f$. A significant difference between the 340 and 110 kDa gels is that the latter complete polymerization upon the end of percolation ($t_p = t_f$), whereas the former continue to polymerize via a second mode of growth following the relation $\Delta G \sim \Delta t^{\alpha_2}$ for $t_p \leq t < t_f$ (Figure 4a).

DOI: 10.1021/acs.langmuir.8b02950
Langmuir XXXX, XXX, XXX−XXX

The modulus plateaus at $G'(t_f)$ after α_2 growth. Taking c = 30 mg mL^{-1}, as is done in the example from the previous section, $G'(t_f) \approx 4000$ Pa corresponds to $\xi \approx 10$ nm; α_2 growth drives gelation to length scales smaller than the protein ($\xi < 2 \times R_G$).

Values of α_2 do not correspond to expectations from percolation models and the fluorescence data in Figure 2 do not exhibit the same multistep growth. Instead, α_2 depends on protein concentration, suggesting that the α_2 growth mechanism is the same for all values of c (Figure 5a). The normal force signature during gelation, which has a local minimum near t_p, suggests that α_1 and α_2 are distinct modes of growth (Figures S2 and S3).

A comparison of time scales among growth of G' and F reveals that α_2 growth does not correspond to dityrosine bond formation (Figure 6). In the 110 kDa gels, the ratio of time

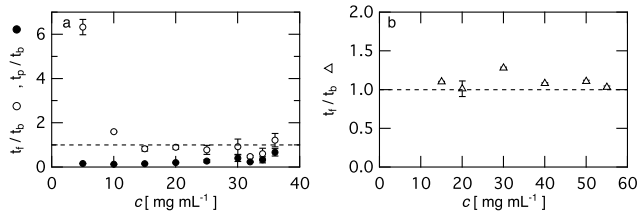

Figure 6. (a) t_f/t_b (○) and t_p/t_b (●) for 340 kDa gels. (b) t_f/t_b (△) for 110 kDa gels. Error bars are a propagation of the uncertainty in t_b and the dashed lines are guides to the eye.

scales $t_f/t_b \sim 1$ signifies that the end of modulus growth/percolation is correlated with the completion of covalent bond formation, unlike the 340 kDa gels in which covalent bonds did not stopped forming by the end of percolation ($t_p/t_b < 1$). In the cases of the lowest values of c for 340 kDa gels, the modulus continues to grow well after the end of covalent bond formation ($t_f/t_b > 1$); in the most extreme case, $t_f/t_b > 6$. Because we expect that the α_2 mechanism is the same for all values of c, α_2 cannot be solely due to dityrosine bonding.

The α_2 growth is likely due to coarsening of interprotein bonds. In the cases with the longest α_2 growth, F slightly decreases after the maximum, suggesting that local chemical changes are occurring that affect the fluorescence spectrum (Figure S5).[36,37] The experimental evidence supported by molecular dynamics simulations has previously shown that tyrosine bonds can act as templates for secondary structure formation of the neighboring amino acids.[24] However, circular dichroism measurements during polymerization do not indicate any changes in the secondary structure (Figure S6). One possible explanation for α_2 is the transitioning from dityrosine to trityrosine bonds. Higher-order tyrosine bonds (>2 tyrosines) have been observed in these enzymatically cross-linked silk systems before.[23] This conversion to higher-order tyrosine bonds could alternatively explain the decrease in F at long times.

CONCLUSIONS

Hydrogels form when horseradish peroxidase enzyme is used to covalently cross-link tyrosines in a reconstituted silk. Whereas covalent bonds are primarily intraprotein at short times, interprotein bonds form a spanning network with a modulus that grows in a manner consistent with the Rouse-like percolation. Depending on the MW of the protein, polymerization either ends after modulus growth, consistent with percolation, or continues following a slower, protein-concentration-dependent coarsening mechanism. Interestingly, for a given protein concentration, both MW distributions polymerize to materials of equivalent G' after α_1 growth. However, the number of bonds as measured through fluorescence differs between the two MW distributions after α_1 growth, with there being more dityrosine bonds per protein fragment for the larger molecular weight distribution gels. Therefore, the molecular weight of the protein influences the efficacy of bonds to contribute to the network modulus.

Neither dityrosine bonding nor the formation of secondary structure within the network appears to establish the secondary growth mode. Regardless of the origin of α_2, its existence indicates that molecular weight changes in silk fibroin do not simply rescale the polymerization dynamics and final mechanical properties. It is possible that this difference in kinetics comes from the contrast in network structure (dangling ends, etc.) that is formed through dityrosine formation. These results further our understanding of enzymatically cross-linked silk hydrogels, progressing toward designing improved silk materials.

ASSOCIATED CONTENT

Supporting Information

The Supporting Information is available free of charge on the ACS Publications website at DOI: 10.1021/acs.langmuir.8b02950.

PDF

AUTHOR INFORMATION

Corresponding Author

*E-mail: dlb76@georgetown.edu.

ORCID

A. Pasha Tabatabai: 0000-0003-0229-7429

David L. Kaplan: 0000-0002-9245-7774

Notes

The authors declare no competing financial interest.

ACKNOWLEDGMENTS

A.P.T. thanks the Meyer Fellowship for funding and Claire McIlroy, Abhay Goyal, and Robin Masurel for helpful discussions. B.P.P., N.R.R., and D.L.K. acknowledge funding from AFOSR: FA9550-17-1-0333.

REFERENCES

(1) Mason, B. N.; Starchenko, A.; Williams, R. M.; Bonassar, L. J.; Reinhart-King, C. A. Tuning 3D Collagen Matrix Stiffness Independently of Collagen Concentration Modulates Endothelial Cell Behavior. *Acta Biomater.* **2013**, *9*, 4635−4644.

(2) Wang, Y.; Kim, H. J.; Vunjak-Novakovic, G.; Kaplan, D. L. Stem cell-based tissue engineering with silk biomaterials. *Biomaterials* **2006**, *27*, 6064−6082.

(3) Zhu, J.; Marchant, R. E. Design properties of hydrogel tissue-engineering scaffolds. *Expert Rev. Med. Devices* **2011**, *8*, 607−626.

(4) Drury, J. L.; Mooney, D. J. Hydrogels for tissue engineering: scaffold design variables and applications. *Biomaterials* **2003**, *24*, 4337−4351.

(5) Yeung, T.; Georges, P. C.; Flanagan, L. A.; Marg, B.; Ortiz, M.; Funaki, M.; Zahir, N.; Ming, W.; Weaver, V.; Janmey, P. A. Effects of substrate stiffness on cell morphology, cytoskeletal structure, and adhesion. *Cell Motil. Cytoskeleton* **2005**, *60*, 24−34.

(6) Zuidema, J. M.; Rivet, C. J.; Gilbert, R. J.; Morrison, F. A. A protocol for rheological characterization of hydrogels for tissue

DOI: 10.1021/acs.langmuir.8b02950
Langmuir XXXX, XXX, XXX−XXX

engineering strategies. *J. Biomed. Mater. Res., Part B* **2014**, *102*, 1063−1073.
(7) Yan, C.; Pochan, D. J. Rheological properties of peptide-based hydrogels for biomedical and other applications. *Chem. Soc. Rev.* **2010**, *39*, 3528−3540.
(8) Doyle, A. D.; Carvajal, N.; Jin, A.; Matsumoto, K.; Yamada, K. M. Local 3D matrix microenvironment regulates cell migration through spatiotemporal dynamics of contractility-dependent adhesions. *Nat. Commun.* **2015**, *6*, No. 8720.
(9) Gardel, M.L.; Nakamura, F.; Hartwig, J.; Crocker, J.; Stossel, T.; Weitz, D. Stress-Dependent Elasticity of Composite Actin Networks as a Model for Cell Behavior. *Phys. Rev. Lett.* **2006**, *96*, No. 088102.
(10) Liu, A. P.; Fletcher, D. A. Biology under construction: in vitro reconstitution of cellular function. *Nat. Rev. Mol. Cell Biol.* **2009**, *10*, 644−650.
(11) Kouwer, P. H. J.; Koepf, M.; Le Sage, V. A. A.; Jaspers, M.; van Buul, A. M.; Eksteen-Akeroyd, Z. H.; Woltinge, T.; Schwartz, E.; Kitto, H. J.; Hoogenboom, R.; Picken, S. J.; Nolte, R. J. M.; Mendes, E.; Rowan, A. E. Responsive biomimetic networks from polyisocyanopeptide hydrogels. *Nature* **2013**, *493*, 651−655.
(12) Jaspers, M.; Dennison, M.; Mabesoone, M. F. J.; MacKintosh, F. C.; Rowan, A. E.; Kouwer, P. H. J. Ultra-responsive soft matter from strain-stiffening hydrogels. *Nat. Commun.* **2014**, *5*, No. 5808.
(13) Adibnia, V.; Hill, R. J. Universal aspects of hydrogel gelation kinetics, percolation and viscoelasticity from PA-hydrogel rheology. *J. Rheol.* **2016**, *60*, 541−548.
(14) Adibnia, V.; Hill, R. J. Viscoelasticity of near-critical silica-polyacrylamide hydrogel nanocomposites. *Polymer* **2017**, *112*, 457−465.
(15) Partlow, B. P.; Hanna, C. W.; Rnjak-Kovacina, J.; Moreau, J. E.; Applegate, M. B.; Burke, K. A.; Marelli, B.; Mitropoulos, A. N.; Omenetto, F. G.; Kaplan, D. L. Highly Tunable Elastomeric Silk Biomaterials. *Adv. Funct. Mater.* **2014**, *24*, 4615−4624.
(16) Partlow, B. P.; Applegate, M. B.; Omenetto, F. G.; Kaplan, D. L. Dityrosine Cross-Linking in Designing Biomaterials. *ACS Biomater. Sci. Eng.* **2016**, *2*, 2108−2121.
(17) Applegate, M. B.; Coburn, J.; Partlow, B. P.; Moreau, J. E.; Mondia, J. P.; Marelli, B.; Kaplan, D. L.; Omenetto, F. G. Laser-based three-dimensional multiscale micropatterning of biocompatible hydrogels for customized tissue engineering scaffolds. *Proc. Natl. Acad. Sci. U.S.A.* **2015**, *112*, 12052−12057.
(18) Yan, L.-P.; Silva-Correia, J.; Ribeiro, V. P.; Miranda-Gonçalves, V.; Correia, C.; da Silva Morais, A.; Sousa, R. A.; Reis, R. M.; Oliveira, A. L.; Oliveira, J. M.; Reis, R. L. Tumor Growth Suppression Induced by Biomimetic Silk Fibroin Hydrogels. *Sci. Rep.* **2016**, *6*, No. 31037.
(19) Rockwood, D. N.; Preda, R. C.; Yucel, T.; Wang, X.; Lovett, M. L.; Kaplan, D. L. Materials fabrication from *Bombyx mori* silk fibroin. *Nat. Protoc.* **2011**, *6*, 1612−1631.
(20) Partlow, B. P.; Tabatabai, A. P.; Leisk, G. G.; Cebe, P.; Blair, D.; Kaplan, D. Silk Fibroin Degradation Related to Rheological and Mechanical Properties. *Macromol. Biosci.* **2016**, *16*, 666−675.
(21) Heinecke, J. W.; Li, W.; Daehnke, H. L.; Goldstein, J. A. Dityrosine, a specific marker of oxidation, is synthesized by the myeloperoxidase-hydrogen peroxide system of human neutrophils and macrophages. *J. Biol. Chem.* **1993**, *268*, 4069−4077.
(22) Michon, T.; Chenu, M.; Kellershon, N.; Desmadril, M.; Guéguen, J. Horseradish Peroxidase Oxidation of Tyrosine-Containing Peptides and Their Subsequent Polymerization: A Kinetic Study. *Biochemistry* **1997**, *36*, 8504−8513.
(23) McGill, M.; Coburn, J. M.; Partlow, B. P.; Mu, X.; Kaplan, D. L. Acta Biomaterialia. *Acta Biomater.* **2017**, *63*, 76−84.
(24) Partlow, B. P.; Bagheri, M.; Harden, J. L.; Kaplan, D. L. Tyrosine templating in the self-assembly and crystallization of silk fibroin. *Biomacromolecules* **2016**, *17*, 3570−3579.
(25) Zhou, C.-Z.; Confalonieri, F.; Jacquet, M.; Perasso, R.; Li, Z.-G.; Janin, J. Silk fibroin: Structural implications of a remarkable amino acid sequence. *Proteins: Struct., Funct., Genet.* **2001**, *44*, 119−122.
(26) Wray, L. S.; Hu, X.; Gallego, J.; Georgakoudi, I.; Omenetto, F. G.; Schmidt, D.; Kaplan, D. L. Effect of processing on silkbased biomaterials: Reproducibility and biocompatibility. *J. Biomed. Mater. Res., Part B* **2011**, *99B*, 89−101.
(27) Lefèvre, T.; Rousseau, M.-E.; Pézolet, M. Protein Secondary Structure and Orientation in Silk as Revealed by Raman Spectromicroscopy. *Biophys. J.* **2007**, *92*, 2885−2895.
(28) Tabatabai, A. P.; Weigandt, K. M.; Blair, D. L. Acid-induced assembly of a reconstituted silk protein system. *Phys. Rev. E* **2017**, *96*, No. 022405.
(29) Rawat, N.; Biswas, P. Size, shape, and flexibility of proteins and DNA. *J. Chem. Phys.* **2009**, *131*, No. 165104.
(30) Tabatabai, A. P.; Kaplan, D. L.; Blair, D. L. Rheology of reconstituted silk fibroin protein gels: the epitome of extreme mechanics. *Soft Matter* **2015**, *11*, 756−761.
(31) Sharma, V.; Jaishankar, A.; Wang, Y.-C.; McKinley, G. H. Rheology of globular proteins: apparent yield stress, high shear rate viscosity and interfacial viscoelasticity of bovine serum albumin solutions. *Soft Matter* **2011**, *7*, 5150−5160.
(32) Russel, W. B.; Saville, D. A.; Schowalter, W. R. *Colloidal Dispersions*; Cambridge University Press, 1989.
(33) Nicell, J. A.; Wright, H. A model of peroxidase activity with inhibition by hydrogen peroxide. *Enzyme Microb. Technol.* **1997**, *21*, 302−310.
(34) Lee, F.; Chung, J. E.; Kurisawa, M. An injectable enzymatically crosslinked hyaluronic acid-tyramine hydrogel system with independent tuning of mechanical strength and gelation rate. *Soft Matter* **2008**, *4*, 880−887.
(35) Guo, L.; Colby, R. H.; Lusignan, C. P.; Howe, A. M. Physical gelation of gelatin studied with rheo-optics. *Macromolecules* **2003**, *36*, 10009−10020.
(36) Lakowicz, J. R. *Principles of Fluorescence Spectroscopy*, 3rd ed.; Springer: US, 2006.
(37) Harms, G. S.; Pauls, S. W.; Hedstrom, J. F.; Johnson, C. K. Fluorescence and rotational dynamics of dityrosine. *J. Fluoresc.* **1997**, *7*, 283−292.

DOI: 10.1021/acs.langmuir.8b02950
Langmuir XXXX, XXX, XXX−XXX